Exploration of a Binding Mode of Benzothiazol-2-yl Acetonitrile Pyrimidine Core Based Derivatives as Potent c-Jun N-Terminal Kinase-3 Inhibitors and 3D-QSAR Analyses

Pooja Sharma and Nanda Ghoshal*

Drug Design, Development and Molecular Modeling Division, Indian Institute of Chemical Biology (CSIR), 4 Raja S.C.Mullick Road, Jadavpur, Kolkata -700032, India

Received February 21, 2006

C-Jun N-terminal kinase (JNK) is a therapeutic target for inhibitors which may provide clinical benefit in the pathogenesis of rheumatoid arthritis (RA) as well as in various apoptosis-related disorders. The benzothiazol-2-yl acetonitrile derivatives, recently reported by Pascale et al. (*J. Med. Chem.* **2005**, *48*, 4596−4607), are the first generation JNK inhibitors of this class. To understand inhibitory mechanisms and elucidate pharmacophoric properties of these derivatives molecular docking and 3D-QSAR studies were performed on a set of 44 compounds. Ligand Fit module of Cerius2 (4.9) was employed to locate the binding orientations of all the compounds within the JNK-3 ATP binding site. A good correlation (r^2=0.810) between the calculated binding free energies (−PMF score) and the experimental inhibitory activities suggests that the identified binding conformations of these potential inhibitors are reliable. Based on the binding conformations, robust and highly predictive 3D-QSAR models were developed with conventional r^2 0.886 and 0.802, full cross-validation r^2 0.980 and 0.788, and predictive r^2 0.965 and 0.968 for MFA and MSA, respectively. The interaction mode was demonstrated taking into consideration inhibitor conformation, hydrogen bonding, and electrostatic interaction. The 3D-QSAR model built in this study will provide clear guidelines for a novel inhibitor design based on the benzothiazole derivatives against JNK-3 for the treatment of inflammatory disorders.

INTRODUCTION

Mitogen-activated protein kinase (MAPK) plays a critical role in the pathogenesis of rheumatoid arthritis (RA), a chronic inflammatory disease marked by cytokine production, synovial lining hyperplasia, and joint destruction along with many important cellular roles including cellular proliferation, apoptosis. Three major MAPK families that differ in their substrate specificity and responses to stress have been identified in vertebrates and have been implicated in RA: c-Jun N-terminal kinase (JNK), extracellular regulating kinase (ERK), and p38 kinase.[1−3] MAPKs phosphorylate selected intracellular proteins, including transcription factors, which subsequently regulate gene expression by transcriptional and post-transcriptional mechanisms. MAPKs are, in turn, activated by phosphorylation at conserved threonine and tyrosine residues by upstream dual-specific MAP kinases (MAPKs), which themselves are activated by MAPKK kinases.[4−7]

The role of cytokines in the pathogenesis of RA is increasingly appreciated,[8] but the signal transduction pathways which determine matrix degradation are only partially understood. Overexpression of matrix metalloproteinases (MMPs), which play a critical role in rheumatoid joint destruction, is of particular interest.[9] MMP production might be regulated, in part, by increased activation of c-Jun N-terminal kinase (JNK) since this MAPK activates key transcription factors involved in MMP gene expression. Several JNK isoforms, encoded by three genes, phosphorylate specific sites (serine 63 and serine 73) on the amino-terminal transactivation domain of c-Jun after exposure to ultraviolet irradiation, growth factors, or cytokines.[10,11] By phosphorylating these sites, the JNKs enhance the transcriptional activity of activator protein (AP-1), a key regulator of MMP production. The JNKs, also termed as stress-activated protein kinases are implicated in cytokine and stress responses. In mammals there are three JNK genes, the ubiquitously expressed *jnk1* and *jnk2* genes and the brain-, heart-, and testis-specific *jnk3* gene.[12−15] It has been reported that JNK blockade suppresses MMP and bone destruction in an animal model of arthritis.[16] Further JNK signaling pathway inhibits neuronal cell death after growth factor withdrawal in vitro, and disruption of the gene encoding the JNK3 isoform in mice prevents kainic acid-mediated cell death of neurons, which strongly suggests a functional role for JNKs in programmed neuronal cell death.[17,18] Mice lacking *jnk1* or *jnk2* exhibit deficits in T-helper (CD4) cell function. Double knockout animals are embryonic lethal, although fibroblasts from these animals are viable in vitro and exhibit a remarkable resistance to radiation-induced apoptosis.[19−22]

Therefore, JNK activity seems to be critical for both programmed cell death and immune response thus therapeutic inhibition of JNK may provide clinical benefit in a wide range of apoptosis-related and inflammatory disorders (e.g. rheumatoid arthritis,[23−25] neurodegenerative diseases, ischemia reperfusion injuries, multiple sclerosis). Recent evidences also support the application of JNK inhibitors in vascular, metabolic, and oncological diseases.[26−30]

Apparently, the interaction mechanism of JNK3 with its inhibitors would be greatly helpful in discovering small

* Corresponding author phone: +91-33-2473-3491 (ext 254); fax: +91-33-2473-0284/5197; e-mail: nghoshal@iicb.res.in.

10.1021/ci060057q CCC: $33.50
Published on Web 05/27/2006

molecule inhibitors for ceasing the function of JNKs. To investigate the mechanism, some three-dimensional structures of the JNK3 itself and its complex with different inhibitors, e.g. the crystal structure of JNK3 in complex with an imidazole-pyrimidine inhibitor (PDB code 1pmn) and with a dihydroanthrapyrazole inhibitor (PDB code 1pmv), have been experimentally determined.[42] These crystal structures provided not only insights into the interaction mechanisms of the JNK3 with the inhibitors but also valuable clues for designing new inhibitors. Protein crystallography has provided a detailed view of the ATP binding site,[42] revealing five distinct subsites with distinct chemical environments and local sequence features that afford an opportunity to develop highly specific kinase inhibitors.

Recently Pascale et al. has identified a novel class of (benzothiazol-2-yl) acetonitrile derivatives as potent and selective JNK-1, -2, -3 inhibitors.[31] SAR studies led to the discovery of the most potent derivative compound **38** of the series (Table 1). It was shown that the potency on JNK3 was improved by the presence of an aromatic group, two carbons away from the aminopyrimidine moiety (Figure 1) and bearing substituents conferring HBA (hydrogen bond acceptor) properties able to reach a second interaction in the ATP binding pocket. The introduction of aminoethyl heteroaromatic substituents allowed access to very potent JNK3 inhibitors with improved physicochemical properties. Compound **38** demonstrated in vivo reduction of tumor necrosis factor-α (TNF-α) production and arthritis severity, confirming the potential of JNK inhibitors to effectively act as anti-inflammatory agents. This compound **38** was established as the most active compound of the series which is moderately selective to JNK3, and it was assumed that its in vivo anti-inflammatory effects are mainly due to the selective inhibition of the JNK isoforms, on the basis of other studies.[32,33] Thus, further structure based drug design study is needed to discover new more selective (benzothiazol-2-yl) acetonitrile inhibitors that are druglike and more potent.

To the best of our knowledge, neither crystal structures of (benzothiazol-2-yl) acetonitrile core based inhibitors in complex with the JNK3 nor 3D-QSAR models are available. Hence we carried out a study to explore the binding mode and orientations of (benzothiazol-2-yl) acetonitrile derivatives against JNK3 using a molecular docking approach. Following the results obtained from the advanced docking program Ligand Fit[40] of Cerius2, 3D-QSAR models were constructed by using approaches of molecular field analysis (MFA) and molecular shape analysis (MSA) in order to provide further insight into the key structural features required to design potential drug candidates of this class.[34] The 3D-QSAR methods are a widely used technique in drug design. However, 3D-QSAR analysis, especially MFA, is sensitive to the spatial orientation of the studied molecules. A successful molecular field analysis depends heavily on the quality of alignment of these molecules. The alignment rules, such as 'atom fit', 'field fit', and 'pharmaophore fit', cannot be used in general because they do not necessarily reflect the topological features of the macromolecule. In fact, it is impossible to construct predictive model if alignment conformations of studied molecules are not their 'active' conformations.[36] Therefore, a new computation method has to be deployed to determine the 'active' conformations correctly for alignment. Undoubtedly, a receptor-based docking technique is an attractive strategy of alignment for MFA, while MSA incorporates spatial molecular similarity data to generate a QSAR equation. Several successful applications of docking alignment with 3D-QSAR have been

Table 1. General Structures and in Vitro JNK3 Inhibitory Activities of the Benzothiazol-2-yl Acetonitrile Pyrimidine Core Based Derivatives Used in 3D-QSAR and Docking Simulations

compd no.[c]	R1	R2	IC_{50}[a]	pIC_{50}[b]
1	H	H	7500	5.12
2	H	NH_2	500	6.30
3	H	Me	950	6.02
4[d]	Me	Me	9400	5.03
5		piperazinyl	6600	5.18
6		4-Me-piperazinyl	6800	5.17
7[d]		morpholinyl	2900	5.54
8		4-OH-piperidinyl	7200	5.14
9	H	$(CH_2)_2N(Me)_2$	1300	5.89
10	H	$(CH_2)_2NH_2$	1490	5.83
11[d]	H	$(CH_2)_2OMe$	820	6.09
12	H	$(CH_2)_2OH$	510	6.29
13	H	$(CH_2)_2$N-piperidinyl	3740	5.43
14	H	$(CH_2)_2$N-morpholinyl	760	6.12
15	H	$(CH_2)_3N(Me)_2$	1644	5.78
16[d]	H	$(CH_2)_3NH_2$	707	6.15
17		$(CH_2)_3OH$	660	6.18
18	H	$(CH_2)_3$N-morpholinyl	407	6.39
19[d]	H	$(CH_2)_3$N-(4-Me-piperazinyl)	473	6.33
20	H	$(CH_2)_3$N-pyrolidinyl-2-one	1340	5.87
21	H	$(CH_2)_3NHMe$	1324	5.88
22	H	CH_2Ph	6500	5.19
23	H	CH_2-pyridin-2-yl	650	6.19
24	H	CH_2-pyridin-3-yl	337	6.47
25	H	CH_2-pyridin-4-yl	340	6.47
26	H	$(CH_2)_2$−Ph-2-F	273	6.56
27	H	$(CH_2)_2$−Ph-3-F	1810	5.74
28	H	$(CH_2)_2$−Ph-4-OH	3500	5.46
29	H	$(CH_2)_2$−Ph-4-OMe	3080	5.51
30	H	$(CH_2)_2$−Ph-4-NH_2	80	7.10
31[d]	H	$(CH_2)_2$−Ph-4-SO_2NH_2	41	7.39
32	H	$(CH_2)_2$−Ph-4-NO_2	600	6.22
33	H	$(CH_2)_2$-indolyl	458	6.34
34[d]	H	$(CH_2)_2$-imidazol-4-yl	80	7.10
35	H	$(CH_2)_2$-imidazol-2N-Me	143	6.84
36	H	$(CH_2)_2$-imidazol-4N-Me	65	7.19
37	H	$(CH_2)_2$-pyridin-2-yl	250	6.60
38	H	$(CH_2)_2$-pyridin-3-yl	120	6.92
39	H	$(CH_2)_2$-N-1,2,4-triazolyl	397	6.40
40	H	$(CH_2)_3$-N-imidazolyl	147	6.83
41	H	$(CH_2)_3$-N-pyrazolyl	583	6.23

compd no.[c]	R3	R4	R5	R6	IC_{50}[a]	pIC_{50}[b]
42	H	H	Br	Cl	350	6.46
43	H	H	H	Cl	250	6.60
44[d]	CF3	H	H	Cl	993	6.00

[a] IC_{50} in vitro JNK3 inhibitory activity. [b] $pIC_{50} = -\log IC_{50}$ (nM). [c] Compounds **1**−**41** correspond to Figure 1, and compounds **42**−**44** correspond to Figure 2. [d] Test set.

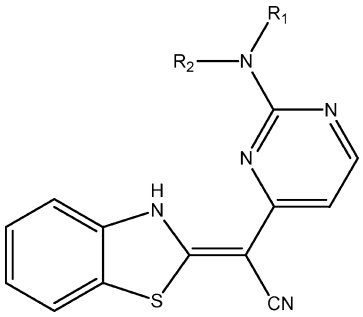

Figure 1.

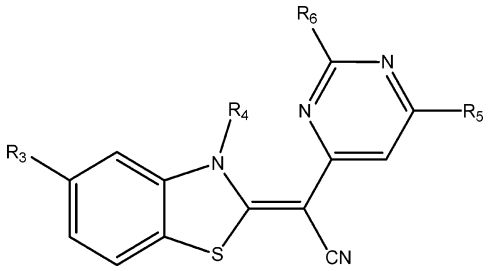

Figure 2.

published.[36−39] Thus the combination of ligand based and receptor based approaches could lead to highly predictive and meaningful QSAR models, able to point out which interaction sites in a binding pocket might be responsible for variance in biological activities.

The results obtained from this study would be useful in both understanding the inhibitory mode of the JNK3 as well as in rapidly and accurately predicting the activities of newly designed inhibitors. These models also provide some beneficial clues in structural modification for designing new inhibitors for the treatment of inflammatory disorders with much higher inhibitory activities against JNK3.

METHODS

Data Set. Forty-four benzothiazol-2-yl acetonitrile pyrimidine core based inhibitors with a common skeleton synthesized by Pascale et al.[31] were employed in this study (Table 1, Figures 1 and 2). The compounds with a nonspecific IC_{50} value (>5000 nM) were not considered for study. The JNK3 inhibition activities for all the compounds were converted into the corresponding pIC_{50} ($-\log IC_{50}$) values, which were used as dependent variables in the MFA and MSA analyses. The pIC_{50} values span a range of 3 log units. The total set of JNK3 inhibitors (44 compounds) were divided into training (36 compounds) and test (8 compounds) sets, which were selected on the basis of structural diversity of molecules possessing activities of wide range.

Molecular modeling software, Cerius2 (version 4.9), on a SGI Fuel workstation with an IRIX 6.5 operating system was used for this study. The 3D-structure of the molecules were modeled by using Build/3d-sketcher module and energy minimized with UNIVERSAL1.02 force field[41] using SMART MINIMIZATION and STANDARD CONVERGENCE with the preferences set to default. The charges were calculated at the beginning, and the charge method used was Gasteiger. To obtain the lowest energy conformation for each molecule energy optimized structures were subjected to dynamics simulation using annealing dynamics with preferences of constant NVE, number of annealing cycles - 5, initial temperature - 300 K, mid cycle temperature - 500 K, temperature increment - 50 K, steps of dynamics per increment - 100, and dynamics time step - 0.001 ps. The above combination of preferences resulted in 2000 steps of dynamics. This was followed by the energy minimization procedure. 8−10 runs were performed for each compound where the maximum number of iterations was 500. The lowest energy structure thus obtained was taken as the final model.

Molecular Docking. To explore the binding mode of benzothiazol-2-yl acetonitrile pyrimidine inhibitors to JNK3, the advanced docking program Ligand Fit[40] of Cerius2 (4.9) was used to automatically dock the ligands to the enzyme. This program gives the user the opportunity to perform both rigid and flexible docking, referring to the conformational state of the ligand. The protein is always considered as rigid, hence, conformational entropy changes (that occur due to conformational flexibility) during the formation of a complex between a protein and a ligand are not considered. The method employs a cavity detection algorithm for detecting invaginations in the protein as candidate active site regions. A shape comparison filter is combined with a Monte Carlo conformational search for generating ligand poses consistent with the active site shape. Candidate poses are minimized in the context of the active site using a grid-based method for evaluating protein−ligand interaction energies. Errors arising from grid interpolation are dramatically reduced using a new nonlinear interpolation scheme. The prediction of the ranking of ligands corresponding to their activity was done by *Ligand scoring*, implemented in the Ligand Fit module, viz. LigScore1&2, PLP1&2, PMF, JAIN, and LUDI scoring functions. The detailed description of algorithms used is presented recently by Venkatachalam et al.[40]

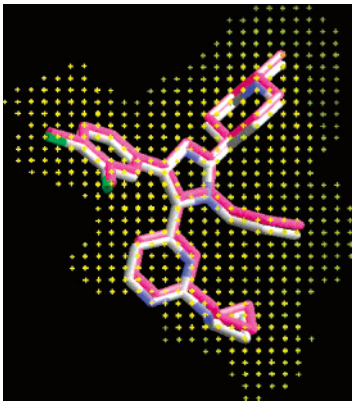

Figure 3. Flexible docking, yielding an RMSD value of 0.368 Å between the starting X-ray conformation of JNK3 inhibitor compound **1a** (nitrogen blue, chlorine green, carbon gray) and the docked pose (pink) presented in the grid of the protein's active site (yellow), with no hydrogen atoms shown.

The whole docking operation in this study could be stated as follows: Reference protein coordinates for docking were taken from the crystal structure of JNK3 in complex with an imidazole-pyrimidine inhibitor (compound **1a**, Figure 3) IC_{50} 7.1 nM; resolution: 2.2 Å (PDB entry 1pmn) from Protein Databank (PDB).[42−44] Charges were assigned to the protein molecule and all the docked ligands using the Cff1.02 force field.[45] The protein/ligand complex was split into two separate models. All solvent molecules were removed, and hydrogen atoms were added using Cerius2 templates for protein residues. The bond order and the number of hydrogen atoms of the ligand were adjusted and saved.

The site search was performed in the shape-based mode. The largest site covered the X-ray ligand conformation and was verified by the location of the redocked X-ray ligand. The site is a collection of grid points which consisted of 3904 grid points in the present case. Most of the proteins can be treated with an eraser size of 5−6 Å as reported in a quantitative investigation of protein−ligand complexes.[40] Therefore, default values of site search preferences (grid resolution 0.5 Å; opening size of the site, 5 Å) were not changed. The ligand (compound **1a**) present in the original

X-ray coordinate file was redocked flexibly within the defined site to the crystal structure of the JNK3 to ensure the accuracy of the site model. Diverse conformations were computed using the Monte Carlo algorithm. To obtain the best results the parameter of maximum best saved conformers was finally set to (*N*save) = 60 with the number of trials being 99 999. Flexible fitting of all 60 conformers and then clustering to remove redundant conformations resulted in the best 10 poses corresponding to 10 diverse conformations and orientations of the ligand. The alignment of X-ray conformation (complexed with JNK3) and the best predicted conformation of compound **1a** yielded RMS deviation of 0.368 Å, shown in Figure 3, indicating that the Ligand fit docking simulation is able to reproduce the X-ray structure. On the basis of this result we decided to set *N*save = 60 for each compound considered for this study.

For all of the training set and test set compounds partial charges were assigned using the Gasteiger calculation. The general protonation state of all the molecules was kept as a noncharged form. Initially during ligand docking, keeping all the compounds completely flexible, we started with the settings of *N*save and *N*MaxTrials as 20 and 15 000, respectively, and Cff1.02 force field; grid resolution 0.5 Å, but could not obtain reasonable results in terms of correlation of experimental activity with any of the scoring functions implemented in *Ligand scoring*. Then the setup conditions were changed to the following preferences: *N*MaxTrials were gradually increased to 30 000, 50 000, and 99 999 with N*save* = 25, 40, and 60, respectively, in order to obtain best results. The ligand-accessible grid was defined such that the minimum distance between a grid point and the protein is 2.0 Å for hydrogen and 2.5 Å for heavy atoms. The grid extends from the defined active site to a distance of 3 Å in all directions. This grid was used to calculate the nonbonded interactions between all the atoms of ligands and protein residues, and nonbonded cutoffs were set to 10 Å. Although the solvation energies could not be explicitly considered during the minimization, the energy calculations were performed with a distance-dependent dielectric constant (default value) to mimic the solvation effect of the inhibitors in the protein environment.[46] Every randomly generated conformation, having an acceptable shape when compared to the site, was oriented by four ways. For each orientation, a rigid body minimization was performed using the steepest descent with 10 iterations. The selected docked conformation was subjected to rigid body minimization for 100 iterations (default) using the BFGS procedure.[34] A flexible fit, wherein the ligand conformational space is explored with different initial poses, was selected in the Monte Carlo simulations. To avoid identical conformations, an RMSD cutoff of 1.5 and a score cutoff of 20 kcal mol^{-1} was maintained while saving the final conformations. The top 60 conformations were saved after rigid body minimizations of 1000 steps. To remove the redundant conformation clustering was performed by using the Complete Linkage method with the specified number of clusters set to 10. The final number of poses obtained for each molecule was 10, thus a total of 440 poses were saved as SD files.

Binding Free Energy Prediction. The scoring function PMF for predicting binding free energy encoded in Ligand Fit was applied to evaluate the binding affinities between the enzyme and the 36 training set inhibitors as well as 8 test set inhibitors. Although Dockscore, Ligscore1 and Ligscore2, PLP1 and PLP2, and LUDI and JAIN scores were also calculated for each of the best 10 saved ligand conformations, in the present study the highest value of the PMF (Potential of Mean Force) score was found to correlate best with the inhibitory activity of these inhibitors against JNK3. Thus it was assumed that binding mode and bioactive conformations of these inhibitors are the same/almost same in both types of JNK3s used during in vitro study by Pascale et al. and in present docking studies. PMF is a statistical analysis approach using 3D structure databases to provide a fast and accurate prediction of protein−ligand binding free energies.[47,48] The scoring function is defined as the sum of the distance-dependent Helmholtz free interaction energies over all interatomic pairs of the protein−ligand complex. The PMF scores are reported in arbitrary energy units with their sign reversed to allow subsequent consensus score calculation. A higher −PMF value indicates a higher protein−ligand binding affinity. The statistical qualities[49] of the linear regression equation were judged by the parameters such as correlation coefficient (r), coefficient of determination (r^2), standard error of estimate (s), and variance ratio (F) at specified degrees of freedom (df).

3D QSAR Studies. To finally explore the specific contributions of electrostatic, steric, and hydrophobic effects for these benzothiazol-2-yl acetonitrile pyrimidine core based JNK3 inhibitors, MFA and MSA (implemented in QSAR module of Cerius2) studies were performed for these inhibitors based on the conformational alignment. The conformation with the strongest predicted binding affinity to the JNK3 for all the compounds was extracted from the optimized inhibitor-JNK3 complex. These conformations were aligned together inside the binding pocket of JNK3 using alignment methods maximum common subgraph (MCSG) for MSA and common substructure (CSS) for MFA studies.

MFA. Molecular field analysis (MFA) is a method for quantifying the interaction energy between a probe molecule and a set of aligned target molecules.[35] A probe molecule is placed at a random location and then moved about a target molecule within a defined 3D grid. At each defined point in the grid, an energy calculation is performed, measuring the interaction energy between the probe and the target molecule. Atoms in the target molecule are fixed, so that intramolecular energy in the target is ignored. When a complete probe map is calculated for each molecule in the target set, energy values for each point in the grid can be reported in columns added to the study table. For a set of structures for which energy fields are generated, some or all of the grid data points can be used as descriptors in generating QSARs and analyzing structure−activity relationships.

The molecules were aligned using the Drug Discovery module[34] of Cerius2. The 'bioactive conformer' of the most active inhibitor **38** for the JNK3 was selected as a standard reference (target model) with which the binding conformations of all training set compounds were aligned through pairwise superpositioning (Figure 4). The Align method - RMS atoms and Align type - Rigid were used. Alignment was performed using CSS which starts with defining a core model (Figure 5), which is a substructure composed of core atoms and substitution sites. Core atoms are those atoms in the core model that exactly match a substructure in all aligned

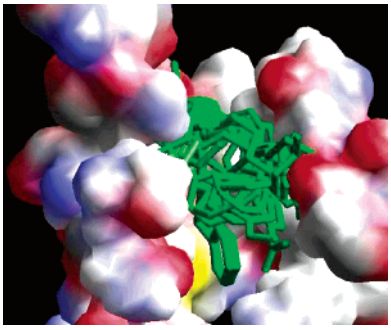

Figure 4. Alignment of training set JNK3 inhibitors (36 compounds shown in green color cylinder model) within the binding pocket of JNK3, in their binding conformations. Surface representation of the active site shows the solvent accessible surface area is colored according to atom types.

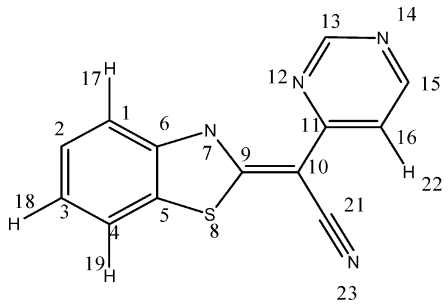

Figure 5. Common substructure of benzothiazole acetonitrile derivatives, used as a template for molecular alignment. The common atoms have been arbitrarily numbered 1−19, 21−23 (it has no relation to the chemical nomenclature system).

models, and substitution sites represent sites where the core model and the matched align models differ. Alignment of structures through pairwise atom superpositioning places all structures under study in the same frame of reference. In the common substructure (core model) 22 atoms are selected for superimposition as shown in Figure 5.

A rectangular field was generated using the probes H^+, OH^-, and CH_3. A grid spacing of 2 Å was used, and fields at 567 points were generated. The energy cutoff was kept at −30 to + 30 Kcal. Only the top 10% of the total descriptors, which explained the maximum variance, were used in the generation of the QSAR. The coordinates of the MFA grid box were (16.336, 3.196, 22.302) and (−32.336, −19.196, −34.302). Due to the large number of points used as independent variables regression analysis was performed using the G/PLS method. The G/PLS method combines the best features of genetic function approximation (GFA) and partial least squares (PLS). GFA is an evolutionary algorithm, which uses a combination of Friedman's multivariate adaptive regression splines (MARS) and Holland's genetic algorithm to evolve a population of equations. In PLS, variables might be overlooked during interpretation or in designing the next experiment even though cumulatively they are very important. This phenomenon is known as loading spread.[34] In GFA, equation models have a randomly chosen proper subset of the independent variables. A generation is the set of models resulting from performing multiple linear regression on each model; the best ones selected become the next generation. Crossover operations are performed on these which take some variables from each of the two models to produce an offspring. In addition, the best model from the previous generation is retained. The linear PLS model finds "new variables" (latent variables) which are linear combinations of the original variables.[34] To avoid overfitting, a strict test for the significance of each consecutive PLS component is necessary, and then stopping when the components are nonsignificant. G/PLS method consisting of 100 000 crossover generations with a population size of 100 was carried out. The optimal number of components was set to 3. The mutation probabilities were kept at system defaults. An energy cutoff of −30.0 kcal/mol was set for both steric and electrostatic contributions. The smoothing parameter, *d*, was set to 1.2 to control the bias in the scoring factors between equations with a different number of terms. The initial equation length value between 5 and 15 is typical for a G/PLS run which is the same as the final equation length.[34,35] In the present case the length of the final equation was fixed to six terms as this value resulted in the best statistical significant QSAR model. PLS analysis was scaled, with all variables normalized to a variance of 1.0. Fields of molecules are represented using grids in MFA, and each energy probe associated with an MFA grid point can serve as input for the calculation of a QSAR. These energies were added to the study table to form new columns headed according to the probe type. A number of QSAR equations were obtained, and each equation was evaluated for statistical significance by cross-validation using leave-one-out (LOO), leave-two-out, and leave-20%-out methods and finally subjected to randomization to obtain the best QSAR model (eq 2). For G/PLS equations, r^2 and the least-squares error (LSE) were taken as statistical measures along with validation parameters cross-validation r^2, predicted residual sum of squares (PRESS), standard deviation of error of prediction (SDEP), and bootstrap r^2 (BS r^2). The predictive ability of the final model was evaluated by external data set validation. The predictive cross-validation coefficient (r^2_{pred}) was calculated as follows

$$r^2_{pred} = 1 - (\sum(Y_{predicted} - Y_{observed})^2 / \sum(Y_{observed} - Y_{mean})^2)$$

where $Y_{predicted}$, $Y_{observed}$, and Y_{mean} are the predicted, observed, and mean of observed values of pIC_{50}, respectively. $\sum(Y_{predicted} - Y_{observed})^2$ is the predictive sum of squares (PRESS), and $\sum(Y_{observed} - Y_{mean})^2$ is the sum of the squared deviations of the dependent variable values from their mean (SD). Both the model development process and finally the developed models were subjected to randomization tests for validation purposes.

MSA. The MSA is a formalism that deals with the quantitative characterization, representation, and manipulation of molecular shape in the construction of a QSAR with the incorporation of spatial molecular similarity data.[50−52] The process has been described by Hopfinger and Burke.[53] The outcome of the MSA process is an optimized QSAR that can be used for activity estimation and ligand evaluation. The QSAR that corresponds to the best fit between observed activities and computed molecular descriptors defines the specific requirements for each MSA task. MSA involves a conformational analysis of the molecules under study and provides input on the relationship of conformational variations with biological activity. In the present case instead of searching the probable binding conformer by using different

approaches implemented in MSA methodology,[34] we have used the best predicted bioactive poses obtained from docking simulation for each molecule under study. Then compound **38** was selected as the candidate shape reference compound to which all the structures in the training set compounds were aligned through pairwise super positioning. The method used for performing the alignment was the maximum common subgroup[34] (MCSG). This method looks at molecules as points and lines and uses the techniques of graph theory to identify patterns. It finds the largest subset of atoms in the shape-reference compound that is shared by all the structures in the study table and uses this subset for alignment. A rigid fit of atom pairings was performed to superimpose each structure so that it overlays the shape-reference compound. MSA descriptors were used to measure molecular shape commonality in their probable binding conformation, while other molecular features were determined by calculating spatial, electronic, and conformational parameters. Thus the following descriptors were used to generate the MSA QSAR model using the G/PLS regression method: (1) MSA descriptors[34] - difference volume (DIFFV), common overlap volume ratio (Fo), RMS to shape reference (ShapeRMS), volume of shape reference (SRVol), noncommon overlap steric volume (NCOSV), and common overlap steric volume (COSV); (2) spatial descriptors - Jurs charged partial surface area descriptors;[54] (3) electronic descriptors - HOMO (highest occupied molecular orbital) energy (in electronvolts) and LUMO (lowest unoccupied molecular orbital) energy; and (4) topological descriptor - molecular shape kappa indices.[55,56] After the calculation of descriptors for the conformers of each training set molecule, conformers were compared to the shape reference compound, and the selected bioactive conformer for each molecule was used for regression analysis. QSAR were generated using the G/PLS method described above. The final QSAR eq 3 was obtained with PLS components (latent variables) three, no. of terms (variables) six, and with scaled PLS analysis. The statistical evaluation for the MSA was performed in the same way as described for MFA.

RESULT AND DISCUSSION

Interaction Modes between the (Benzothiazol-2-yl) Acetonitrile based Inhibitors and the JNK3. Figure 4 depicts the aligned binding conformations of the (benzothiazol-2-yl) acetonitrile inhibitors in the binding pocket of the JNK3, which were derived from the docking simulations followed by energy minimizations. Thirty-six training set and 8 test set compounds were docked inside the active site of the energy minimized form of JNK3 using Ligand Fit. The originally reported[57] structure of unphosphorylated JNK3 in complex with an ATP analogue and the structure used for this study is substantially identical, with an RMSD of 0.61 Å on Cα atoms. Protein crystallography has provided a detailed view of the ATP binding site. The catalytic domain comprises an N-terminal domain spanning residues 45−149 and 379−400 and a C-terminal domain spanning residues 150−211 and 217−374. As expected, inhibitors used in this study bind in the ATP binding site like the docked ligand in the crystallographic complex. Binding modes of the most active compound **38** has been shown in Figure 6.

The benzothiazole acetonitrile moiety interacts with **Met 149** through hydrogen bonding. An intramolecular hydrogen bond forming between the "NH" group of the benzothiazole moiety and one of the nitrogens of the pyrimidine ring seems important for interaction with the JNK3 ATP binding pocket. It was observed by Pascale[31] et al. that the replacement of the benzothiazole moiety and the cyano group by benzoimidazole and ethyl ester, respectively, results in a drastic loss of activity. The hydrogen bonding to the main chain nitrogen mimics the hydrogen bond made by ATP, and it has been shown in kinases, in general, to be essential for inhibitor binding.[58,59] Most of the active compounds (e.g., **26**, **34**, **38**, **2**, **29**, **37**, **41**, **21**, **32**, **33**, **19**, **13**, **40**, **22**) of the series show the same type of interaction with the protein, involving the main chain nitrogen and oxygen atoms of **Met 149** in the linker region (the bond distance is 1.591 Å for compound **38**, Figure 6). The presence of the pyrimidine "NH" was found to be very important for binding as this part enables the ring to act as a hydrogen bond acceptor and interacts with the glycine rich loop (Gly71-Val78) of the catalytic domain which is the phosphate binding area. For example, compound **38** interacts via hydrogen bonding with **Ile 70** (bond distance 1.789 Å, Figure 6), while compounds **26**, **27**, **29**, and **37** interact with **Gly 71**, compounds **2** and **21** interact with **Ser 72**, and compounds **15** and **17**−**20** interact with **Val 78**, through their pyrimidine NH region.

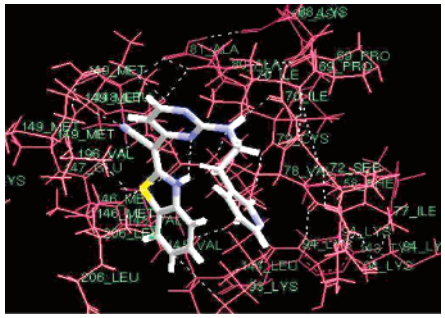

Figure 6. The interacting mode and binding conformation of compound **38** with JNK3 active site. The inhibitor and the important residues for inhibitor-protein interaction are represented by cylinder (nitrogen blue, sulfur yellow, carbon gray, hydrogen white) and stick models (magenta), respectively. The white dashed lines denote the hydrogen bonds.

It was observed that the flexibility of substituents at aminopyrimidine moiety (Figure 1) play a very important role in the binding process to protein amino acid residues. Major differences have been observed between energy states of initial lowest energy conformation and final best docked conformations of all the compounds. For instance, compound **38** had a lowest energy state, obtained by energy minimization coupled with the dynamic simulation process with a total energy of 55.6 kcal/mol. In this energy state it had a dihedral angle of the pyrimidine "NH" having a value of 3.6° which is very close to normal sp^2 hybridization. After docking the molecule in JNK3 active site its energy level was found to be higher with a value of 78.83 kcal/mol for its best predicted docked pose. This probable bioactive conformation possesses the dihedral angle of 91.4° for the pyrimidine "NH" which is quite higher than the normal value. Interestingly, it was found that for all data set molecules among the 10 best binding poses out of 60 saved docked conformations, the orientation having the value of this angle higher than 85° showed a higher free energy of binding than that of other

conformations. This common factor in almost all probable bioactive conformations for an entire data set of molecules indicates that the dihedral angle (value around 85°−110°) of the pyrimidine "NH" plays an important role in the binding of molecules to the phosphate binding area of the catalytic domain. Work is under progress to experimentally validate the above results. It was observed that the compounds with the length of the linker two to three carbons, between the pyrimidine and the polar group (R_2, Figure 1), are able to reach the interaction which comes under the glycine rich loop (Gly71-Val78). This was further validated by designing a compound with an increased length of the linker chain to four carbon atoms in compound **38**, which showed a loss in binding free energy as well as in predicted activity (details vide MFA discussion). These data validate that the length of the linker, between the pyrimidine and polar group (R_2), are important for interaction. Additionally, this linker seems to provide optimum flexibility to molecules in order to make the above interaction feasible. Further, the benzothiazole ring has been found to interact with **Lys 93** by noncovalent bonding in a hydrophobic region of the binding pocket which consists of the side chains of Ala91, Lys93, Leu206, Ile124, Ile126, Leu144, and Met146 and the main chain atoms of Leu144-Met146 and Ala91-Lys93.[57]

Correlation between Binding Free Energy and Inhibitory Activity. The automated molecular docking may produce several options of binding conformation for each inhibitor. The Monte Carlo conformational search trials were increased to 99 999 from an initial value of 15 000 trials to obtain the best orientations of binding within the ATP binding pocket of JNK3. Thus the binding conformations of compounds in the training set and the test set corresponding to the highest binding affinity (highest value of scoring function −PMF) with JNK3 were selected as the most possible binding (bioactive) conformations. The predicted free energies (scoring function −PMF) of binding for all the molecules with JNK3 and the corresponding experimental pIC_{50} values are listed in Table 2.

A good correlation was found between the PMF score and the pIC_{50} via a linear regression analysis eq 1, and this relationship is graphically shown in Figure 7

$$-\log IC_{50} = 1.49953 + 0.063874*(-PMF) \qquad (1)$$

where *N*obs = 44, $r^2 = 0.810$, $r = 0.891$, $F = 163.54$ (df 1, 42), intercept = 1.8091, $s = 0.278$, PRESS = 2.966, Dep SD = 14.709, leave-one-out CV $r^2 = 0.800$, leave-two-out CV $r^2 = 0.799$, leave-20%-out CV $r^2 = 0.788$.

r^2 is the correlation coefficient, CV r^2 is the cross-validation coefficient, F is the testing factor of the reliability which is the variance ratio at specified degrees of freedom (df), s is the standard error of estimate, and Dep SD is the standard deviation of error of prediction.

The correlation coefficient (r^2) is 0.810. With the theoretical F value at a probability level of 0.01 (df 1, 42) being 4.07, the variance ratios of eq 1 are significant at the 0.05 level of confidence, indicating stability of the regression coefficients. Further this model was cross-validated by leave-one-out CV r^2= 0.800, leave-two-out CV r^2 =0.799, and leave-20%-out CV $r^2 = 0.788$ methods. This rather high and almost constant value of CV r^2 shows that this regression model is statistically significant and stable. These results and good correlation between −PMF and pIC_{50} demonstrates that the binding conformations and binding mode of the (benzothiazol-2-yl) acetonitrile inhibitors to the JNK3 used in the present study are reasonable. The binding modes of these inhibitors in the JNK3 active site are consistent with earlier studies,[57−59] regarding binding of other JNK3 inhibitors to its ATP binding pocket, indicating that it was possible to successfully discover the most probable binding conformation for each inhibitor. Therefore, a more quantitative explanation to the structure−activity relationship of the inhibitory mechanism of these inhibitors can be given.

Table 2. Binding Free Energies (−PMF) of Benzothiazol-2-yl Acetonitrile Pyrimidine Derivatives JNK3 Inhibitors, Calculated via Docking Simulations

compd no.	pIC_{50}[a]	−PMF	compd no.	pIC_{50}[a]	−PMF
1	5.12	53.8	**23**	6.19	69.5
2	6.30	71.2	**24**	6.47	76.31
3	6.02	66.97	**25**	6.47	73.52
4[b]	5.03	55.60	**26**	6.56	83.48
5	5.18	58.90	**27**	5.74	71.00
6	5.17	56.20	**28**	5.46	51.00
7[b]	5.54	59.70	**29**	5.51	65.67
8	5.14	54.50	**30**	7.10	86.86
9	5.89	66.62	**31**[b]	7.39	81.14
10	5.83	72.27	**32**	6.22	65.70
11[b]	6.09	69.36	**33**	6.34	72.87
12	6.29	75.23	**34**[b]	7.10	78.00
13	5.43	62.84	**35**	6.84	84.60
14	6.12	72.42	**36**	7.19	79.40
15	5.78	70.24	**37**	6.60	79.17
16[b]	6.15	69.4	**38**	6.92	88.38
17	6.18	74.51	**39**	6.40	72.76
18	6.39	77.64	**40**	6.83	75.98
19[b]	6.33	76.99	**41**	6.23	68.00
20	5.87	71.32	**42**	6.46	68.60
21	5.88	72.10	**43**	6.60	76.34
22	5.19	58.30	**44**[b]	6.00	70.10

[a] $pIC_{50} = -\log IC_{50}$ (nM). [b] Test set.

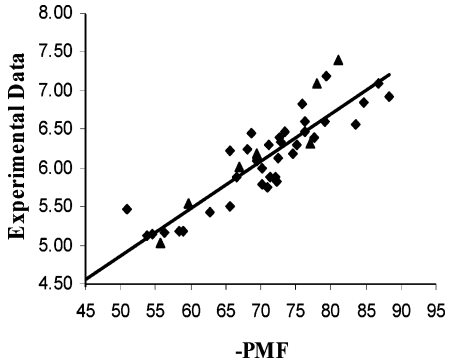

Figure 7. Correlation between the predicted binding free energies (−PMF scores) and the experimental activities (pIC_{50}): (■) compounds of the training set and (▲) compounds of the test set.

MFA Model. The MFA model was generated using the CSS alignment of the most probable binding conformations obtained from the above results. MFA evaluates the energy between a probe and a molecular model at a series of points defined by a rectangular grid and depends heavily on the quality of alignment of these molecules. G/PLS analysis was carried out for the 36 best binding conformations of the training set, and the best equation obtained is eq 2. The predicted activities from eq 2, for both training set and test set molecules, are listed in Table 3 along with their observed activities. The best equation with alignment of predictive

Table 3. Experimental Activities (pIC_{50}) and Predicted Activities (G/PLS Pred) by MFA and MSA, for the Training Set and Test Set Molecules

		MFA		MSA	
compd no.	pIC_{50}[a]	G/PLS Pred	δ[b]	G/PLS Pred	δ[b]
1	5.12	5.60	−0.48	5.45	−0.33
2	6.30	5.98	0.31	6.17	0.12
3	6.02	6.16	−0.14	6.08	−0.06
4[c]	5.03	5.13	−0.10	5.17	−0.14
5	5.18	5.03	0.15	5.34	−0.16
6	5.17	5.22	−0.05	5.01	0.15
7[c]	5.54	5.36	0.18	5.45	0.09
8	5.14	5.28	−0.14	5.15	−0.01
9	5.89	5.97	−0.08	5.80	0.08
10	5.83	5.86	−0.03	6.00	−0.17
11[c]	6.09	6.12	−0.03	6.18	−0.09
12	6.29	6.17	0.11	6.26	0.02
13	5.43	5.40	0.02	5.53	−0.10
14	6.12	6.03	0.08	5.53	−0.10
15	5.78	5.67	0.10	6.16	−0.04
16[c]	6.15	6.21	−0.06	6.19	−0.04
17	6.18	6.26	−0.08	5.85	0.32
18	6.39	6.41	−0.02	6.12	0.26
19[c]	6.33	6.18	0.15	6.23	0.10
20	5.87	5.94	−0.07	5.85	0.01
21	5.88	5.808	0.07	6.07	−0.19
22	5.19	5.20	−0.01	6.05	−0.86
23	6.19	6.34	−0.19	6.32	−0.13
24	6.47	6.41	0.05	6.29	0.17
25	6.47	6.38	0.09	6.26	0.20
26	6.56	6.55	0.01	6.81	−0.25
27	5.74	5.77	−0.03	5.75	−0.01
28	5.46	5.27	0.18	5.93	−0.47
29	5.51	5.59	−0.08	6.09	−0.58
30	7.10	7.24	−0.14	6.86	0.23
31[c]	7.39	7.18	0.21	7.62	0.23
32	6.22	6.37	−0.15	6.14	0.07
33	6.34	6.29	0.05	6.69	−0.35
34[c]	7.10	7.21	−0.11	6.94	0.15
35	6.84	6.67	0.16	7.21	−0.37
36	7.19	7.36	−0.17	6.47	0.71
37	6.60	6.35	0.24	6.08	0.51
38	6.92	7.01	−0.09	6.66	0.35
39	6.40	6.08	0.31	6.43	−0.03
40	6.83	6.76	0.06	6.66	0.16
41	6.23	6.21	0.02	6.40	−0.17
42	6.46	6.29	0.17	6.35	0.11
43	6.60	6.40	0.19	6.53	0.06
44[c]	6.00	6.03	−0.03	6.09	−0.09

[a] $pIC_{50} = -\log IC_{50}$ (nM). [b] δ residual values. [c] Test set.

binding conformations obtained from docking results is as follows

$$\text{activity} = 6.10229 + 0.355547*\text{“CH}_3\text{/610”} - 20.1449*\text{“CH}_3\text{/585”}\wedge 2 - 0.116882*<-22.2654 - \text{“H}^+\text{/190”}> - 0.001427*\text{“H}^+\text{/693”}\wedge 2 - 1.81171*<- 0.236049-\text{“CH}_3\text{/308”}> \quad (2)$$

where *N*obs = 36, generalized $r^2 = 0.886$, LOO CV $r^2 = 0.980$, BS $r^2 = 0.845$, and outliers = 1.

Statistical details for MFA model (eq 2) are given in Table 4. 'H$^+$/ 693', 'CH$_3$/ 585', ..., and so on, are the probe energies, and the numbers correspond to their spatial positions at the rectangular points 693 and 585, respectively (shown in Figure 9). The terms in angle brackets, < >, are spline terms which are used in the equation only when their value is greater than zero, * is the sign of multiplication (all the terms being multiplied by their respective coefficients).

Table 4. Statistical Indexes of MFA and MSA 3D-QSAR Models Based on (Benzothiazol-2-yl) Acetonitrile Derivatives Binding Conformations, Using G/PLS Method with Validation Tests

S.no.	trials	MFA	MSA
r^2 (conventional)		0.886	0.802
F test		24.537	18.435
LSE		0.084	0.077
BS r^2 (± SD)		0.845 ± 0.018	0.815 ± 1.121
PRESS		4.651	4.931
SDEP		1.378	0.586
CV r^2 (leave-one-out)	2	0.980	0.788
CV r^2 (leave-two-out)	2	0.876	0.762
CV r^2 (leave 20% out)	5	0.801	0.723
r^2_{pred}		0.965	0.968
randomization test confidence level 99%			
R from nonrandom model		0.881	0.821
no. of random trials		99	99
mean value of *R* from random trials ± SD		0.532 ± 0.164	0.587 ± 0.259

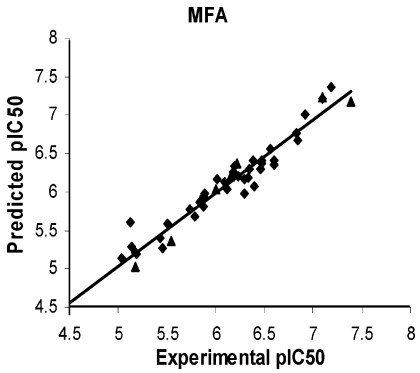

Figure 8. The predicted activities versus the experimental activities (pIC_{50}) of the benzothiazol-2-yl acetonitrile compounds via MFA: (■) compounds of the training set and (▲) compounds of the test set.

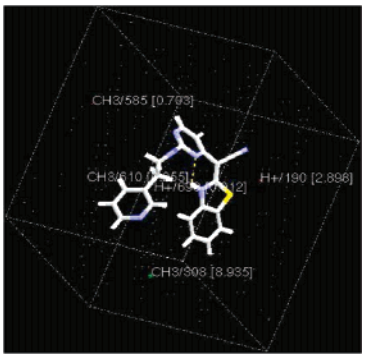

Figure 9. Compound 38 enclosed inside the rectangular grid with 3D points of the (MFA) QSAR eq 2.

The term *N*obs means the number of data points; r^2 is the square of the correlation coefficient, which is used to describe the goodness of fit of the data of the study compounds to the QSAR model. BS r^2 is the average squared correlation coefficient calculated during the validation procedure. Removal of outliers was not considered as the model was statistically good.

The scatter plot of actual versus predicted activities, for both training set and test set molecules, obtained from eq 2 is shown in Figure 8.

To determine the model's reliability and significance, both full cross-validation procedures[34] and randomization were

performed. Standard cross-validation in G/PLS encompasses only the optimization of regression coefficients; it does not encompass optimization of the choice of descriptors. That is, the regression model is validated only for the specific subset of descriptors obtained from G/PLS. In contrast, full cross-validation encompasses the entire algorithm, including both the choice of descriptors and the optimization of regression coefficients.[62] Here full cross-validation was performed by LOO, leave-two-out, and leave-20%-out methods, and the r^2 values were found to be 0.980, 0.876, and 0.801, respectively. The equation was further tested for statistical significance by randomization. The randomization was done by repeatedly permuting the dependent variable set (i.e., the mean activity data). A decrease in the value of r^2 indicates a good model as equations are generated with scrambled activity data during randomization.[62] Randomization was performed at a 99% confidence level (99 random trials) for each QSAR model, using the same preferences that were earlier used to obtain the particular QSAR. Equation 2 exhibited a confidence level of 99%, and mean values of random *R*'s were found to be 0.532. Additionally, the model had a very good r^2_{pred} of 0.965 in an external data set validation with eight test set compounds.

MFA attempts to postulate and represent the essential features of a receptor site from the aligned common features of the molecules that bind to it.[60] MFAs are quantitative and differ from qualitative pharmacophore models;[61] the former tries to capture essential information about the receptor, while the latter only captures information about the similarity of the compounds that bind. MFA eq 2 specifies the regions where variations in the structural features, for different compounds in the training set, would lead to increased or decreased activities.

The presence of CH_3/308 as a spline term with a negative coefficient indicates that the JNK3 inhibitory activity is maximum when steric hindrance is minimum at the first position of the benzothiazole ring (Figure 9, compound **38**). It means that the presence of a bulky group or any other substitution at the first position of the benzothiazole ring will reduce the biological activity. As found in the binding modes of these inhibitors this part of the ring forms noncovalent bonds with Lys 93 in the JNK3 active site, thus any type of hindrance would interfere in binding. This observation is consistent with the study of Pascale et al.[31] since the presence of CF_3 at the above position showed the reduction of potency in compound **44** as compared to that in compound **43** (Table 1). Further the presence of $(H^+/693)^2$ with a negative coefficient close to the vicinity of NH of the aminopyrimidine moiety (Figure 9) shows that the stronger the electron donating capacity of the substituents on the pyrimidine moiety, the weaker the potency. Any substituent that enhanced the electron-deficient character of the pyrimidine ring increased the potency of the inhibitors within this series (see Table 1). For example, compound **12** [$R_2 = (CH_2)_2$-OH] has lesser electron donating capacity than that of compound **11** [$R_2 = (CH_2)_2$OMe], which shows a higher predicted activity [**12**>**11**] (Table 3). This observation validates the experimental data. The presence of probe CH_3/610 with a positive coefficient at the linker carbon atom chain between the pyrimidine and the polar group indicates its moderate (two or three C atom) value would increase the activity.[31] This was validated by designing a compound with an increased length of the linker chain to four carbon atoms [$R_2 = (CH_2)_4$-pyridin-3-yl] in compound **38**, which showed a decrease in the predicted activity (G/PLS Pred=5.27) as well as the predicted free energy of binding (−PMF=68) as compared to that of compound **38**.

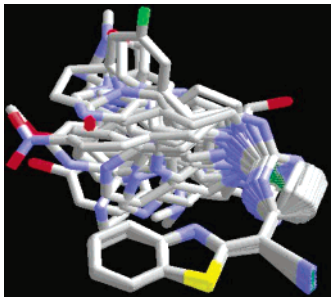

Figure 10. Superimposition of the best probable binding conformations of 36 benzothiazol acetonitrile derivatives extracted from docking analysis with JNK3 and their alignment using the 'MCSG' method. The atoms of inhibitors are depicted as cylinder models (nitrogen blue, oxygen red, sulfur yellow, chlorine green, fluorine light green, and carbon gray).

MFA describes a self-consistent field around the molecules that can explain activity. The MFA generated model in this study was statistically significant and used to correctly predict the activities of a set of training and test molecules (Tables 3 and 4) indicating that these models could be useful tools to design potent inhibitors for JNK3.

MSA Model. In an attempt to find out spatial molecular similarity data along with some important parameters for these inhibitors, an MSA-QSAR study was performed for the same training set of 36 molecules with their probable 'bioactive' conformations. A view of aligned molecules studied is shown in Figure 10.

Each study molecule was aligned to the shape reference compound **38** using the MCSG search. This places all the molecules in the same frame of reference, allowing for the calculation of shape descriptors. In addition to the shape descriptors, other molecular descriptors were also considered while generating the QSAR equation (as detailed in method section). The predicted activities, obtained from best 3D QSAR model generated (eq 3), for both training set and test set molecules, are listed in Table 3 along with their experimental activities. The scatter plot of actual versus predicted activities, for both training set and test set molecules, obtained from eq 3 are shown in Figure 11.

The QSAR equation generated by G/PLS method is given as

$$\text{activity} = 1.66192 - 0.5577*\langle\text{"HOMO"}-3.90773\rangle - 31.9182*\langle 0.9000839\text{-"Jurs-PPSA-3"}\rangle - 2.67369*\langle\text{"Jurs-RNCG}-5.33143\rangle - 5.5728*\text{"Kappa-1"} + 85.382*\text{"Jurs-FPSA-3"}-0.206589*\langle\text{"NCOSV"}-27.4672\rangle \quad (3)$$

where *N*obs = 36, generalized $r^2 = 0.802$, cross-validated (LOO) $r^2 = 0.788$, BS $r^2 = 0.815$, and there are no outliers.

Statistical details for this MSA model (eq 3) are given in Table 4. The cross- validated r^2 values by LOO, leave-two-out, and leave-20%-out methods were found to be 0.788, 0.762, and 0.723, respectively. The final model eq 3 was subjected to a randomization test with 99 random trials. It exhibited a 99% confidence level on randomization with mean values of random *R*'s of 0.587. The model had a good

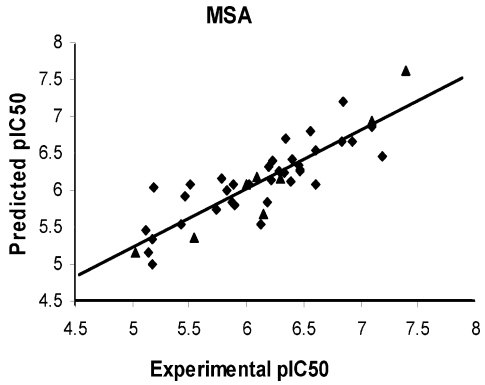

Figure 11. The predicted activities versus the experimental activities (pIC_{50}) of the benzothiazol-2-yl acetonitrile compounds using MSA: (■) compounds of the training set and (▲) compounds of the test set.

r^2_{pred} of 0.968 for eight test set compounds. The equation consists of one shape descriptor, one topological, one electronic, and three spatial descriptors. An analysis of the correlation matrix showed that no significant correlation among the independent variables exists.

In eq 3 the presence of a negative coefficient of noncommon overlap steric volume (NCOSV) indicates that its higher value is detrimental to the binding affinity. This means the presence of steric substituents larger than those present in the shape-reference compound lowers the binding affinity. For example, compounds **5**, **27**, and **9**−**11** have a comparatively larger value of NCOSV and show lesser inhibitory activity to that of the shape-reference compound **38**. The negative coefficient of Jurs-RNCG (the relative negative charge i.e., the charge of the most negative atom divided by the total negative charge) indicates that the higher value of the relative negative charge is detrimental to the binding affinity to JNK3. Higher values of Jurs-RNCG are observed for compounds **5**, **8**, and **22** having piperazinyl, 4-OH-piperidinyl, and $(CH_2)_3Ph$ substituents, respectively, at the R_2 position (Table 1, Figure 1), and they show lesser inhibitory activity as compared to that of the shape reference compound. The descriptor Jurs fractional positive surface area- 2 (Jurs FPSA-3) [(partial positive surface area * total charge on the molecule)/(total molecular surface area)] with a positive coefficient indicates that its higher value will increase the activity. Compounds **7**, **13**, **44**, and **32** having a lesser value of Jurs FPSA-3 show lesser potency than that of the most active compound **38** (Table 1). The negative coefficient for Kappa-1 in eq 3 shows that the higher degree of cyclicity within the molecule is detrimental for activity. For example, compounds **5**−**8** with cyclic amines as substituents on the pyrimidine moiety show very poor binding and less potency. The negative coefficient of HOMO indicates that the more nucleophilicity of the molecules will decrease the binding affinity. This is in accordance with the observation of Pascale et al.[31] that the stronger the electron donating capacity of the substituents on the pyrimidine moiety, the weaker the potency ($N(Me)_2$ < NHMe < $NHNH_2$ < Cl) on JNK3. These QSAR studies (MFA and MSA) are complementary and establish the molecular basis for the inhibition of JNK3; therefore, they can be used as a guide for developing molecules with better activity.

Validation of the 3D-QSAR Models. The summary of statistical details of MFA and MSA 3D-QSAR models are given in Table 4. A high value of CV r^2 alone, however, is insufficient criterion for a QSAR model to be robust, and although a good randomization[62] result ensures no chance correlations, it does not guarantee a good predictive model.[63,64] In view of several recent findings, the emphasis has been given for the validation on an external test set.[65−67] The predictive power of the constructed MFA and MSA models was therefore validated with a set of eight test molecules, representing a wide variety in structure and activity where CV is cross-validated r^2, r^2_{pred} is the test set predictive r^2, LSE is the Least Square Error, BS is bootstrap r^2, and SDEP is the standard deviation of error of prediction.

The predicted pIC_{50}'s with the QSAR models are in good agreement with the experimental data (within a statistically tolerable error range) with a correlation coefficient of r^2_{pred} = 0.965 and 0.968 for MFA and MSA models, respectively (Table 4). The test set results indicate that the MFA and MSA models could be reliably used in new benzothiazol-2-yl acetonitrile pyrimidine inhibitor design for developing better drugs against RA.

Docking versus 3D QSAR. The success of molecular field and shape similarity analysis is completely determined by the conformations chosen for the superimposition of the studied molecules. The MFA method is very sensitive to the spatial orientation of the compounds as it captures essential information about the receptor site from the aligned set of compounds. For instance, in MFA and docking studies (Figures 9 and 6, respectively) the presence of probe **H^+**/**190** in the vicinity of the benzothiazole acetonitrile moiety and hydrogen bonding of the acetonitrile group with residue **Met 149**; probe **CH_3**/**308** in the vicinity of the first position of the benzothiazole ring and its noncovalent interaction with residue **Lys 93** within hydrophobic region; and probe **H^+**/**693** close to the vicinity of NH of the aminopyrimidine moiety which interacts through hydrogen bonding with residue **Ile 70** show the complementarities of the topology of the binding pocket and optimized 3D field points. In general, we observed a nice agreement between the 3D field grid points and the positions of particular amino acid residues in the active site. In MSA, spatial molecular similarity data based on 3D alignment of binding spatial orientations (obtained from docking) of the training set compounds toward one another represents the relative differences in the binding geometry at the active site. These inhibitors with their probable binding arrangement within an active site resulted in a highly significant MSA model which is useful for activity estimation and ligand evaluation. Hence, docking methodology which provides bioactive conformations of the molecules under study is complementary to 3D-QSAR method.

CONCLUSION

Molecular docking and 3D-QSAR studies, carried out to explore the binding mechanism of benzothiazol-2-yl acetonitrile pyrimidine core based inhibitors to JNK3, resulted in highly predictive 3D-QSAR models for designing new JNK3 inhibitors for the treatment of inflammatory disorders. The binding conformations of 44 benzothiazol-2-yl acetonitrile pyrimidine molecules inside the ATP binding pocket of JNK3 were determined, and their binding free energies were predicted by molecular docking. The binding models of the

inhibitors clearly show the interaction mode by which these inhibitors bind to the JNK3 active site. The binding free energies of these compounds to the JNK3, estimated by a statistical analysis approach, Potential of Mean Force (PMF), were found to have a good correlation with the experimental inhibitory potencies. Based on the binding conformations from molecular docking, highly predictive MFA and MSA models were developed. These models match well with the 3D topology of the binding site of JNK3. The reliability of the models was verified by predicting the activity of the compounds in the test set. The 3D-QSAR results revealed some important sites, where steric, electrostatic (donor/acceptor), and hydrophobic modifications would significantly affect compounds' bioactivities, thus providing useful clues to design novel inhibitors of JNK3 with promising activity. Finally these results, together with the good correlations between the inhibitory activities and binding free energies predicted by Ligand fit, demonstrate the power of the combined docking-QSAR approach to explore the probable binding conformations of compounds at the active site of the protein target and further develop reliable quantitative models for rational drug design.

ACKNOWLEDGMENT

The authors thank the Council for Scientific and Industrial Research (CSIR), New Delhi, India for financial assistance. We thank the Accelrys support group for their valuable suggestions.

REFERENCES AND NOTES

(1) Lander, H. M.; Jacovina, A. T.; Davis, R. J.; Tauras, J. M. Differential activation of mitogen-activated protein kinases by nitric oxide-related species. *J. Biol. Chem.* **1996**, *271*, 19705−19709.

(2) Lo, Y. Y. C.; Wong, J. M. S.; Cruz, T. F. Reactive oxygen species mediate cytokine activation of c-jun NH_2-terminal kinase. *J. Biol. Chem.* **1996**, *271*, 15703−15707.

(3) Schwarzschild, M. A.; Cloe, R. L.; Hyman, S. E. Glutamate, but not dopamine, stimulates stress-activated protein kinase and AP-1- mediated transcription in striatal neurons. *J. Neurosci.* **1997**, *17*, 3455−3466.

(4) Robinson, M. J.; Cobb, M. H. Mitogen-activated protein kinase pathways. *Curr. Opin. Cell. Biol.* **1997**, *9*, 180−185.

(5) Seger, R.; Krebs, E. G. The MAPK signaling cascade. *FASEB J.* **1995**, *9*, 726−735.

(6) Fanger, G. R.; Gerwins, P.; Widmann, C.; Jarpe, M. B.; Johnson, G. L. MEKKs, GCKs, MLKs, PAKs, TAKs, and tpls: upstream regulators of the c-Jun amino-terminal kinases? *Curr. Opin. Genet. Dev.* **1997**, *7*, 67−76.

(7) Hibi, M.; Lin, A.; Smeal, T.; Minden, A.; Karin, M. Identification of an oncoprotein- and UV-responsive protein kinase that binds and potentiates the c-Jun activation domain. *Genes Dev.* **1993**, *7*, 2149−2160.

(8) Firestein, G. S. In *Rheumatoid arthritis*; Ruddy, S. Ed.; Scientific American Inc.: New York, U.S.A. *Sci. Am. Med.* **1998**, *15*, 2.1−2.14.

(9) Firestein, G. S.; Paine, M. M.; Littman, B. H. Gene expression (collagenase, tissue inhibitor of metallproteinases, complement, and HLA-DR) in rheumatoid arthritis and osteoarthritis synovium: Quantitative analysis and effect of intra-articular corticosteroids. *Arthritis Rheum.* **1991**, *34*, 1094−1105.

(10) Devary, Y.; Karin, M. The mammalian ultraviolet response is triggered by activation of Src tyrosine kinases. *Cell* **1992**, *71*, 1081−1091.

(11) Kallunki, T.; Su, B.; Tsigelny, I.; Sluss, H. K.; Derijard, B.; Moore, G.; Davis, R.; Karin, M. JNK2 contains a specificity-determining region responsible for efficient c-Jun binding and phosphorylation. *Genes. Dev.* **1994**, *8*, 2996−3007.

(12) Kyriakis, J. M.; Banerjee, P.; Nikolakaki, E.; Dai, T.; Rubie, E. A.; Ahmad, M. F.; Avruch, J.; Woodgett, J. R. The stress-activated protein kinase subfamily of c-Jun kinases. *Nature* **1994**, *369*, 156−160.

(13) Tibbles, L. A.; Woodgett, J. R. The stress-activated protein kinase pathways. *Cell. Mol. Life Sci.* **1999**, *55*, 1230−1254.

(14) Ip, Y. T.; Davis, R. J. Signal transduction by the c-Jun N-terminal kinase (JNK) \320 from inflammation to development. *Curr. Opin. Cell. Biol.* **1998**, *10*, 205−219.

(15) Gupta, S.; Barrett, T.; Whitmarsh, A. J.; Cavanagh, J.; Sluss, H. K.; Derijard, B.; Davis, R. J. Selective interaction of JNK protein kinase isoforms with transcription factors. *EMBO J.* **1996**, *15*, 2760−2770.

(16) Zuoning, H.; David, L. B.; Lufen, C. c-Jun N-terminal kinase is required for metalloproteinase expression and joint destruction in inflammatory arthritis. *J. Clin. Inves.* **2001**, *108*(1), 73−81.

(17) Anna, C. M.; Marcie, A. G.; Alie, N. B.; Kevin, M. W.; Ernest, K. J.; Carol A. M.; Becky A. B.; James P. F.; Thelma A.; Yuzuru M.; Nicola T. N.; Craig A. D. Motoneuron apoptosis is blocked by CEP-1347-(KT7515), a novel inhibitor of the JNK signaling pathway. *J. Neurosci.* **1998**, *18*, 104−111.

(18) Watson, A.; Eliers, A.; Lallemand, D.; Kyriakis, J.; Rubin, L. L.; Ham, J. Phosphorylation of c-Jun is necessary for apoptosis induced by survival signal withdrawal in cerebellar granule neurons. *J. Neurosci.* **1998**, *18*, 751−762.

(19) Dong, C.; Yang, D. D.; Wysk, M.; Whitmarsh, A. J.; Davis, R. J.; Flavell, R. A. Defective T cell differentiation in the absence of Jnk1. *Science* **1998**, *282*, 2092−2095.

(20) Yang, D. D.; Conze, D.; Whitmarsh, A. J.; Barrett, T.; Davis, R. J.; Rincon, M.; Flavell, R. A. Differentiation of CD4+ T cells to Th1 cells requires MAP kinase JNK2. *Immunity* **1998**, *9*, 575−585.

(21) Sabapathy, K.; Hu, Y.; Kallunki, T.; Schreiber, M.; David, J. P.; Jochum, W.; Wagner, E. F.; Karin, M. JNK2 is required for efficient T-cell activation and apoptosis but not for normal lymphocyte development. *Curr. Biol.* **1999**, *9*, 116−125.

(22) Tournier, C.; Hess, P.; Yang, D. D.; Xu, J.; Turner, T. K.; Nimnual, A.; Bar-Sagi, D.; Jones, S. N.; Flavell, R. A.; Davis, R. J. Requirement of JNK for stress-induced activation of the cytochrome *c*-mediated death pathway. *Science* **2000**, *288*, 870−874.

(23) Han, Z.; Boyle, D. L.; Aupperle, K. R.; Bennett, B.; Manning, A. M.; Firestein, G. S. Jun N-terminal kinase in rheumatoid arthritis. *J. Pharmacol. Exp. Ther.* **1999**, *291*, 124−130.

(24) Han, Z.; Boyle, D. L.; Chang, L.; Bennett, B.; Karin, M.; Yang, L.; Manning, A. M.; Firestein, G. S. c-Jun N-terminal kinase is required for metalloproteinase expression and joint destruction in inflammatory arthritis. *J. Clin. Invest.* **2001**, *108*, 73−81.

(25) Han, Z.; Chang, L.; Yamanishi, Y.; Karin, M.; Firestein, G. S. Joint damage and inflammation in c-Jun N-terminal kinase 2 knockout mice with passive murine collagen-induced arthritis. *Arthritis Rheum.* **2002**, *46*, 818−823.

(26) Lin., A. Activation of the JNK signaling pathway: Breaking the brake on apoptosis. *Bioessays* **2003**, *25*, 17−24.

(27) Manning, A. M.; Davis, R. J. Targeting JNK for therapeutic benefit: from junk to gold? *Nat. Rev. Drug Discovery* **2003**, *2*, 554−565.

(28) Resnick, L.; Fennell, M. Targeting JNK3 for the treatment of neurodegenerative disorders. *Drug Discovery Today* **2004**, *9*, 932−939.

(29) Bennett, B. L.; Satoh, Y.; Lewis, A. J. JNK: a new therapeutic target for diabetes. *Curr. Opin. Pharmacol.* **2003**, *3*, 420−425.

(30) Kennedy, N. J.; Davis, R. J. Role of JNK in tumor development. *Cell Cycle* **2003**, *2*, 199−201.

(31) Pascale, G.; Isabelle J. E.; Vittoria A.; Steve, A.; Yves, C.; Montserrat, C.; Christian, C.; Dennis, C.; Rocco, C.; Denise, G.; Serge, H.; Anthony, N.; Cedric, S.; Pierre, A. V.; Gotteland, J. P. Design and Synthesis of the first generation of Novel Potent, Selective, and *in vivo* Active (Benzothiazol-2-yl) acetonitrile Inhibitors of the c-Jun N-Terminal Kinase. *J. Med. Chem.* **2005**, *48*, 4596−4607.

(32) Ferrandi, C.; Ballerio, R.; Gaillard, P.; Giachetti, C.; Carboni, S.; Vitte, P. A.; Gotteland, J. P.; Cirillo, R. Inhibition of c-Jun N-terminal kinase decreases cardiomyocyte apoptosis and infarct size after myocardial ischemia and reperfusion in anaesthetized rats. *Br. J. Pharmacol.* **2004**, *142*, 953−960.

(33) Carboni, S.; Hiver, A.; Szyndralewiez, C.; Gaillard, P.; Gotteland, J. P.; Vitte, P. A. AS601245 (1,3-benzothiazol-2-yl(2-[[2-(3-pyridinyl)-ethyl]amino]-4 pyrimidinyl) acetonitrile): a c-Jun NH2- terminal protein kinase inhibitor with neuroprotective properties. *J. Pharmacol. Exp. Ther.* **2004**, *310*, 25−32.

(34) *MSI Cerius2 Version 4.9, Molecular simulations*; Accelrys Inc.: 9685 Scranton Rd., San Diego, CA 92121, U.S.A., [online]; http:// www.msi.com.

(35) (a) Hirashima, A.; Eiraku, T.; Kuwano, E.; Eto, M. Three-Dimensional Molecular Field Analyses of Agonists for Tyramine Receptor which Inhibit Sex-Pheromone Production in *Plodia* interpunctella. *I.E.J.M.D.* **2003**, *2*, 511−526. (b) Ghoshal, N.; Mukherjee, P. 3-D-QSAR of N-substituted 4-amino-3, 3-dialkyl-2(3H)-furanone GABA receptor modulators using molecular field analysis and receptor surface modelling study. *Bioorg. Med. Chem. Lett.* **2004**, *14*, 103−109. **(c)** Bhattacharya, P.; Leonard, J. T.; Roy, K. Exploring 3D-QSAR of thiazole and thiadiazole derivatives as potent and selective human

adenosine A_3 receptor antagonists. *J. Mol. Model. Comput. Chem.* **2005**, *11*, 516−524.
(36) (a) Spippl, W. Development of biologically active compounds by combining 3D QSAR and structure-based design methods. *J. Comput.-Aided Mol. Des.* **2002**, *16* (11), 825−830. (b) Sippl, W.; Höltje, H. D. Structure-based 3D-QSAR—merging the accuracy of structure based alignments with the computational efficiency of ligand-based Methods. *J. Mol. Struct.* (*THEOCHEM)* **2000**, *503*, 31−50. **(**c**)** Folkers, G.; Merz, A.; Rognan, D. In *3D-QSAR in Drug Design- Theory, Methods and Applications*; Kubinyi, H., Ed.; ESCOM Science Publishers BV: Leiden, 1993; pp 583−618. (d) Klebe, G.; Abraham, U. On the prediction of binding properties of drug molecules by comparative molecular field analysis. *J. Med. Chem.* **1993**, *36*, 70−80.
(37) Chen, H.; Li, Q.; Yao, X.; Fan, B.; Yuan, S.; Panaye, A.; Doucet, J. P. 3D-QSAR and Docking Study of the Binding Mode of Steroids to Progesterone Receptor in Active Site. *QSAR Comb. Sci.* **2003**, *22*, 604−613.
(38) Ma, X.; Zhang, X.; Tan, J.; Chen, W.; Wang, C. Exploring binding mode for styrylquinoline HIV-1 integrase inhibitors using comparative molecular field analysis and docking studies. *Acta Pharmacol. Sin.* **2004**, *25*, 950−958.
(39) Liu, G.; Zhang, Z.; Luo, X.; Shen, J.; Liu, H.; Shen, X.; Chen, K.; Jiang, H. Inhibitory mode of indole-2-carboxamide derivatives against HLGPa: molecular docking and 3D-QSAR analyses. *Bioorg. Med. Chem.* **2004**, *12*, 4147−57.
(40) Venkatachalam, C. M.; Jiang, X.; Oldfield, T.; Waldman, M. Ligand Fit: a novel method for the shape-directed rapid docking of ligands to protein active sites. *J. Mol. Graphics Modell.* **2003**, *21*(4), 289−307.
(41) Rappe, A. K.; Casewit, C. J.; Colwell, K. S.; Goddard, W. A.; Skiff, W. M., III UFF, A full periodic table force field for molecular mechanics and molecular dynamics simulations. *J. Am. Chem. Soc.* **1992**, *114*, 10024−10035.
(42) Scapin, G.; Patel, S. B.; Lisnock, J.; Becker, J. W.; Lograsso, P. V. The Structure of Jnk3 in Complex with Small Molecule Inhibitors: Structural Basis for Potency and Selectivity. *Chem. Biol.* **2003**, *10*, 705−712.
(43) Laskowski, R. A. PDB sum: summaries and analyses of PDB structures**.** *Nucleic. Acids Res.* **2001**, *29*(1), 221−2.
(44) RCSB PDB, [online]; http://www.rcsb.org.
(45) Maple, J. R.; Hwang, M. J.; Stockfish, T. P.; Dinur, U.; Waldman, M.; Ewig, C. S.; Hagler, A. T. Derivation of class II force fields. I. Methodology and quantum force field for the alkyl functional group and alkane molecules. *J. Comput. Chem.* **1994**, *15*, 161−182.
(46) (a) Mehler, E. L.; Solmajer, T. Electrostatic effects in proteins: comparison of dielectric and charge models. *Protein Eng.* **1991**, *4*, 903−910. (b) Leach, A. R. In *Molecular Modelling: Principles and Applications*; Pearson Edu. Ltd., England, 2001; Chapter 4, pp 165−252.
(47) Muegge, I.; Martin, Y. C.; Hajduk, P. J.; Fesik, S. W. Evaluation of PMF scoring in docking weak ligands to the FK506 binding protein. *J. Med. Chem.* **1999**, *42*(14), 2498−503.
(48) Irene, N.; Mitchell, J. B. O.; Alexander, A.; Thornton, J. M. Evaluation of a Knowledge-Based Potential of Mean Force for Scoring Docked Protein−Ligand Complexes. *J. Comput. Chem.* **2001**, *22(*7), 673−688.
(49) *Statistica 6.0*; Stat Soft Inc.: 2300 East 14th Street, Tulsa OK 74104, U.S.A.
(50) Hopfinger, A. J.; Tokarski, J. S. In *Practical Applications of Computer-Aided Design*; Charifson, P. S., Ed.; Marcel Dekker: New York, 1997; pp 105−164.
(51) Burke, B. J.; Hopfinger, A. J. 1-(Substituted-benzyl) imidazole-2(3H)-thione inhibitors of dopamine beta.-hydroxylase. *J. Med. Chem.* **1990**, *33*, 274−281.
(52) Burke, B. J.; Hopfinger, A. J. In *Molecular Similarity*; Johnson, M. A., Maggiora, G. M., Eds.; John Wiley and Sons: New York, 1990; pp 11−EnDash73.
(53) Hopfinger, A. J.; Burke, B. J. In *Concepts and Applications of Molecular Similarity*; Johnson, M. A., Maggiora, G. M., Eds.; John Wiley and Sons: New York, 1990; p 173.
(54) Stanton, D. T.; Jurs, P. C. Development and use of charged partial surface area structural descriptors in computer assisted quantitative structure property relationship studies. *Anal. Chem.* **1990**, *62*, 2323−2329.
(55) Hall, L. H.; Kier, L. B. The Molecular Connectivity Chi Indexes and Kappa Shape Indexes in Structure−Property Relations. In *Reviews of Computational Chemistry*; Boyd, D., Lipkowitz, K., Eds.; VCH Publishers: 1991; Chapter 9, pp 367−422.
(56) Kier, L. B.; Hall, L. H. The Kappa Indices for Modeling Molecular Shape and Flexibility. In *Topological Indices and Related Descriptors in QSAR and QSPR;* Devillers, J., Balaban, A. T., Eds.; Gordon and Breach Reading, U.K., 1999; pp 455−490.
(57) Xie, X.; Yong, G.; Fox, T.; Coll, J. T.; Fleming, M. A.; Markland, W.; Caron, W.; Caron, P. R.; Wilson, K. P.; Michael, S. S. S. Crystal structure of JNK3: a kinase implicated in neuronal apoptosis. *Structure* **1998**, *6*, 983−991.
(58) Toledo, L. M.; Lydon, N. B.; Elbaum, D. The structure-based design of ATP-site directed protein kinases inhibitors. *Curr. Med. Chem.* **1999**, *6*, 775−805.
(59) Boehm, J. C.; Adams, J. L. New inhibitors of p38 kinase. *Expert Opin. Ther. Pat.* **2000**, *10*, 25−37.
(60) Hahn, M. Receptor Surface Models. 1. Definition and Construction. *J. Med. Chem.* **1995**, *38*, 2080−2090.
(61) Hirashima, A.; Eiraku, T.; Kuwano, E.; Taniguchi, E.; Eto, M. Three-dimensional pharmacophore hypotheses of octopamine receptor responsible for the inhibition of sex-pheromone production in *Plodia interpunctella*. *Internet Electron. J. Mol. Des.* **2002**, *1*, 37−51.
(62) (a) Wold, S.; Eriksson, L. In *Chemometric Methods in Molecular Design;* Waterbeemd, H. V. D., Ed.; VCH Publishers: New York, 1995; pp 309−318. (b) Fan, Y.; Shi, L. M.; Kohn, K. W.; Pommier, Y.; Weinstein, J. N. Quantitative Structure-Antitumor Activity Relationships of Camptothecin Analogues: Cluster Analysis and Genetic Algorithm-Based Studies. *J. Med. Chem.* **2001**, *44*, 3254−3263.
(63) Golbraikh, A.; Tropsha, A. Beware of q^2. *J. Mol. Graphics Modell.* **2002**, *20*, 269−276.
(64) Golbraikh, A.; Shen, M.; Xiao, Z.; Xiao, Y. D.; Lee, K. H.; Tropsha, A. Rational selection of training and test sets for the development of validated QSAR models. *J. Comput.-Aided. Mol.* Des. **2003**, *17* (2−4), 241−53.
(65) (a) Wold, S.; Martens, H.; Wold, H. In *The Multivariate Calibration Problem in Chemistry solved by the PLS Method*; Proc. Conf. Matrix Pencils; 1983. (b) In *Lecture Notes in Mathematics 973*; Ruhe, A., Kågstro, B. M., Eds.; Springer-Verlag: Heidelberg, 1982; pp 286−293.
(66) Wold, S. Cross validatory estimation of the number of components in factor and principal components models. *Technometrics* **1978**, *20*, 397−405.
(67) Saxena, A. K.; Prathipati, P. Comparison of MLR, PLS and GA-MLR in QSAR analysis. *SAR QSAR Environ. Res.* **2003**, *14*, 433−446.

CI060057Q